Blucher Mechanical Engineering Proceedings
May 2014, vol. 1 , num. 1
www.proceedings.blucher.com.br/evento/10wccm

ACCELERATED PARTITIONED FLUID-STRUCTURE INTERACTION USING SPACE-MAPPING

T. P. Scholcz[1], A. H. van Zuijlen[1], H. Bijl[1]

[1] Faculty of Aerospace Engineering, Delft University of Technology (t.p.scholcz@tudelft.nl)

Abstract. *The focus of this paper is on acceleration of strong partitioned coupling algorithms for fluid-structure interaction. Strong partitioned coupling requires the solution of a coupled problem at each time step during the simulation. Hereto, an interface residual is defined such that the kinematic and dynamic interface conditions on the fluid-structure interface are satisfied when it amounts to zero. Subsequently, the coupled problem is formulated as a minimization problem of the interface residual which can efficiently be performed using Newton's method. However, Newton's method cannot be applied when the fluid and structure solvers are considered black-boxes since the Jacobian of the interface residual is not available. For this reason, Quasi-Newton methods were developed that approximate either the Jacobian or the inverse Jacobian of the interface residual directly from input/output information.*

In this contribution we present a new algorithm that uses a technique from multi-fidelity optimization – called space-mapping – to efficiently perform the minimization of the interface residual. The space-mapping technique exploits a computationally inexpensive low-fidelity model in order to accelerate an expensive high-fidelity model using black-box information only. The space-mapping algorithm is applied to the supersonic panel flutter problem in order to demonstrate its effectiveness. The speedup – defined with respect to a Quasi-Newton algorithm – is found to be 1-1.5 for typical time step sizes. It is expected that higher speedups can be obtained when problems are considered that require strong coupling as the time step decreases, e.g. due to the added mass effect when the structure is in interaction with an incompressible fluid.

Keywords: *Fluid-structure interaction, Partitioned, Strongly coupled, Space-mapping, Quasi-Newton*

1. Introduction

Fluid-structure interaction plays a major role in many fields. Examples are flutter or buffeting of wings, bio-fluids in deformable vessels or wind interaction with cable stayed bridges. However, the computational cost related to high fidelity models – especially when the interaction is strong – limits their direct use in industry.

The aim of this research is to accelerate the sub-iteration process necessary to obtain the transient solution of a high fidelity fluid-structure interaction problem in a partitioned

fashion using off-the-shelf lower fidelity fluid models. There is an increasing demand for coupling algorithms that are efficient, stable and compatible with standard CFD solvers as well [4,10]. Space mapping [5,6] is a technique from multi-fidelity optimization that aims to accelerate the iterative process – necessary to find a high fidelity solution – by exploiting a computationally cheap lower fidelity model using black-box information only. We will present a new algorithm that uses space mapping to accelerate the sub-iteration process of a fluid-structure interaction problem and study the *speedup* with respect to a common Quasi-Newton algorithm: the Quasi-Newton Inverse Least Squares (QN-ILS) algorithm [2,4,10] . The QN-ILS algorithm uses the inverse least squares method to approximate the inverse Jacobian of the interface residual that needs to be minimized in order to obtain the high fidelity solution. The QN-ILS method has succesfully been applied to strongly coupled FSI problems [2,4,10].

Approximation of a Jacobian from input/output information is also required in the Aggressive Space Mapping (ASM) algorithm [5,6]. Hereto, mainly *Broyden's method* has been used in the space mapping community [5,6]. Broyden's method uses information of two recent iterates to approximate the Jacobian from input/output information. The method has also been used in the FSI community [7,8] and in the first work on space mapping accelerated algorithms for FSI [9]. In contrast to Broyden's method, the inverse least squares method uses information from several previous iterates and is therefore often more succesfull. In this contribution the inverse least squares method is chosen to approximate the inverse of the space mapping Jacobian. This results in the Aggressive Space Mapping Inverse Least Squares (ASM-ILS) algorithm defined in section 3.3.

We apply the ASM-ILS algorithm to a simple linear academic test problem: the supersonic panel flutter problem [9,12]. We give the panel an initial deflection and obtain the free response with the Newmark-β time-integration scheme [13]. The speedup is subsequently studied for different parameter settings and time step sizes in section 5.

2. Problem formulation

A typical FSI model consists of a fluid model defined on a deformable domain Ω_f which is in interaction with a structure model defined on Ω_s. The Arbitrary Langrangian Eulerian (ALE) formulation is used for the fluid in order to take into account the movement of the structure which is modeled using a pure Lagrangian formulation. The fluid domain and structure domain both have a fluid-structure interaction interface Γ_I^f and Γ_I^s which are identical, such that both domains are coupled [1]. We use the method of lines: A spatial discretization technique is used to obtain the semi-discrete systems of equations describing the dynamics of each physical system before a time-integration procedure is employed.

Let the vector $\mathbf{v}$ denote the discrete state vector of the fluid in Ω_f and vector $\mathbf{u}$ the discrete state vector of the structure in Ω_s at the new time level t^{n+1}. Hiding the dependency on the solution of previous time levels, the coupled problem at time step t^{n+1} is formulated as [2];

$$\mathbf{r}^f(\mathbf{v}; \xi_x(\mathbf{u})) = \mathbf{0} \quad \mathbf{v} \in \mathbb{R}^{N_f} \tag{1}$$

$$\mathbf{r}^s(\mathbf{u}; \xi_y(\mathbf{v})) = \mathbf{0} \quad \mathbf{u} \in \mathbb{R}^{N_s}. \tag{2}$$

Here, $\mathbf{r}^f$ denotes the residual of the discrete fluid equations and $\mathbf{r}^s$ the residual of the discrete structure equations. The function $\xi_x : \mathbb{R}^{N_s} \rightarrow \mathbb{R}^{N_I}$ maps the structural state vector $\mathbf{u} \in \mathbb{R}^{N_s}$ to the interface displacement vector $\mathbf{x} \in \mathbb{R}^{N_I}$, hence $\mathbf{x} = \xi_x(\mathbf{u})$. The function $\xi_y : \mathbb{R}^{N_f} \rightarrow \mathbb{R}^{N_I}$ maps the fluid state vector $\mathbf{v} \in \mathbb{R}^{N_f}$ to the interface pressure $\mathbf{y} \in \mathbb{R}^{N_I}$, hence $\mathbf{y} = \xi_y(\mathbf{v})$.

Given a certain interface displacement vector $\mathbf{x}$ the following sequence of function evaluations

$$\mathbf{y} = \xi_y(\mathbf{v}) \quad \text{for} \quad \mathbf{v} = \arg \min_{\mathbf{v} \in \mathbb{R}^{N_f}} ||\mathbf{r}^f(\mathbf{v}; \mathbf{x})||, \tag{3}$$

defines the *the fluid operator* $\mathcal{F} : \mathbb{R}^{N_I} \rightarrow \mathbb{R}^{N_I}$

$$\mathbf{y} = \mathcal{F}(\mathbf{x}). \tag{4}$$

Evaluating the fluid operator requires solution of the minimization problem in (3) up to a certain tolerance ϵ_f and the evaluation of the map ξ_y to find the interface pressure from the fluid state vector. The minimization of $\mathbf{r}^f$ is in general performed with a CFD solver and requires the adaption of a grid due to the deformation of the fluid domain.

Likewise, given an interface pressure $\mathbf{y}$ the sequence of function evaluations

$$\mathbf{x} = \xi_x(\mathbf{u}) \quad \text{for} \quad \mathbf{u} = \arg \min_{\mathbf{u} \in \mathbb{R}^{N_s}} ||\mathbf{r}^s(\mathbf{u}; \mathbf{y})||, \tag{5}$$

defines the *structure operator* $\mathcal{S} : \mathbb{R}^{N_I} \rightarrow \mathbb{R}^{N_I}$

$$\mathbf{x} = \mathcal{S}(\mathbf{y}). \tag{6}$$

Evaluation of the structure operator requires the solution of the minimization problem in Eq. (5) up to a certain tolerance ϵ_s and evaluation of the map ξ_x to find the interface displacement from the structure variables. The kinematic and dynamic interface conditions require continuity of the interface displacement/velocity and force equilibrium on the fluid-structure interface. These conditions are satisfied when [2,3,4]

$$\mathcal{R}(\mathbf{x}) = \mathbf{0} \quad \text{with} \quad \mathcal{R}(\mathbf{x}) = \mathcal{S} \circ \mathcal{F}(\mathbf{x}) - \mathbf{x}, \tag{7}$$

where $\mathcal{R} : \mathbb{R}^{N_I} \rightarrow \mathbb{R}^{N_I}$ is the *interface residual* function.

Strong coupling algorithms aim to minimize the interface residual $\mathcal{R}$ to a certain tolerance ϵ_I using a minimum number of (expensive) fluid operator evaluations. We aim to obtain the solution $\mathbf{x}^*$ given by

$$\mathbf{x}^* = \arg \min_{\mathbf{x} \in \mathbb{R}^{N_I}} ||\mathcal{R}(\mathbf{x})||, \tag{8}$$

as efficiently as possible.

When $\epsilon_f = \epsilon_s = \epsilon_I = 0$ we find $\mathbf{u} = \mathbf{u}^*$ and $\mathbf{v} = \mathbf{v}^*$ satisfying Eq. (1) and (2) and the unique interface displacement and pressure are found from $\mathbf{x}^* = \xi_x(\mathbf{u}^*)$ and $\mathbf{y}^* = \xi_y(\mathbf{v}^*)$ respectively. We can think of Eq. (8) as an optimization problem that needs to be solved at every time step of the simulation. Methods that were originally developed for multi-fidelity optimization can be applied to the minimization problem in Eq. (8) and this can possibly result in efficient coupling algorithms. In this contribution we investigate the application of *space mapping* [5,6,14] to minimize the interface residual in Eq. (8).

3. Space Mapping

Space mapping is an optimization technique conceived by Bandler [14] and initially applied to problems in the field of electromagnetics. Since the underlying principles of space mapping are quite general, it provides a framework that can be applied in many other areas as well [5]. A space mapping algorithm requires the definition of a computationally inexpensive low-fidelity model (hereafter named the coarse model) and a space mapping function. These are the topics of sections 3.1 and section 3.2 respectively. When the space mapping function is approximated by a linearization and the Jacobian is approximated from input/output information the Aggressive Space Mapping (ASM) algorithm results. The ASM algorithm is outlined in section 3.3 and applied to the minimization problem (8).

3.1. Coarse fluid model

Let $\tilde{\mathbf{r}}^f(\tilde{\mathbf{v}}, \mathbf{z})$ denote the residual of the discrete fluid equations describing a simplified fluid model. The simplified fluid model has the interface displacement $\mathbf{z} \in \mathbb{R}^{N_I}$ as an argument. Given an interface displacement $\mathbf{z}$, the sequence of function evaluations

$$\tilde{\mathbf{y}} = \xi_y(\tilde{\mathbf{v}}) \quad \text{for} \quad \tilde{\mathbf{v}} = \arg \min_{\tilde{\mathbf{v}} \in \mathbb{R}^{\tilde{N}_f}} ||\tilde{\mathbf{r}}^f(\tilde{\mathbf{v}}; \mathbf{z})|| \tag{9}$$

defines the coarse fluid operator $\tilde{\mathbf{y}} = \tilde{F}(\mathbf{z})$, such that the coarse fluid-structure interaction problem becomes

$$\tilde{\mathcal{R}}(\mathbf{z}) = \mathbf{0} \quad \text{with} \quad \tilde{\mathcal{R}}(\mathbf{z}) = \mathcal{S} \circ \tilde{\mathcal{F}}(\mathbf{z}) - \mathbf{z}. \tag{10}$$

In Eq. (10) we only use a coarse fluid operator since we assume that a fluid operator evaluation is far more expensive than a structure operator evaluation. Although a simplified structure operator could also be used in Eq. (10) this is not considered in this contribution.

The solution of the coarse fluid-structure interaction problem is given by

$$\mathbf{z}^* = \arg \min_{\mathbf{z} \in \mathbb{R}^{N_I}} ||\tilde{\mathcal{R}}(\mathbf{z})||. \tag{11}$$

The minimization in (11) – up to a tolerance $\tilde{\epsilon}_I$ – is assumed to be computationally very inexpensive when compared to the minimization of the fine model residual in Eq. (8). In order to use coarse model information to accelerate the minimization of the interface residual of the high fidelity model we need to somehow relate the coarse residual function to the fine residual function. Since the coarse and fine residuals are defined in different function spaces this is accomplished by a space mapping function.

3.2. Space mapping function

The fine and coarse fluid model differ and therefore it holds that $\mathbf{x}^* \neq \mathbf{z}^*$. Yet, the models are similar since they aim to model the same phenomenon. In order to quantify the misalignment between the fine and coarse model we define a misalignment function on the fluid-structure interface

$$r(\mathbf{z}, \mathbf{x}) = ||\tilde{\mathcal{R}}(\mathbf{z}) - \mathcal{R}(\mathbf{x})||, \tag{12}$$

using a suitable norm. For a given $\mathbf{x}$ it is useful to know which $\mathbf{z}$ yields the best approximation to $\mathcal{R}$, hence with the smallest misallignent r. Finding the best $\mathbf{z}$ for a given $\mathbf{x}$ defines the space mapping function $\mathcal{P} : \mathbb{R}^{N_I} \rightarrow \mathbb{R}^{N_I}$

$$\mathbf{z} = \mathcal{P}(\mathbf{x}) = \arg \min_{\mathbf{z} \in \mathbb{R}^{N_I}} r(\mathbf{z}, \mathbf{x}). \tag{13}$$

In order to evaluate the space mapping function numerically a second "auxiliary" fluid-structure interaction problem needs to be solved with the coarse fluid operator. This problem can be solved with fixed point iterations or a Quasi-Newton algorithm and defines the *inner* method. Evaluation of the space mapping function requires a single expensive evaluation of the fine fluid operator and several cheap evaluations of the coarse fluid operator to perform the mapping. An example of the numerical evaluation of the space mapping function (using fixed point iterations) is given in algorithm 2. The space mapping function can be used to conveniently reformulate the rootfinding problem (7) which forms the basis of the Aggressive Space Mapping algorithm discussed in the next section.

3.3. The Aggressive Space Mapping algorithm

The following definition is cited from [5]

Definition 1 *A space mapping function $\mathcal{P}$ is called a perfect mapping iff $\mathbf{z}^* = \mathcal{P}(\mathbf{x}^*)$.*

Substituting $\mathbf{x}^*$ into the space mapping function defined by Eq. (13) and using definitions (8), (11) and (12) it follows that $\mathcal{P}$ is a perfect mapping. It is now possible to apply a Quasi-Newton method to the new rootfinding problem

$$\mathcal{K}(\mathbf{x}) = \mathbf{0} \quad \text{with} \quad \mathcal{K}(\mathbf{x}) = \mathcal{P}(\mathbf{x}) - \mathbf{z}^*, \tag{14}$$

with $\mathcal{K} : \mathbb{R}^{N_I} \rightarrow \mathbb{R}^{N_I}$, which is the *outer* method. This results in the Aggressive Space Mapping (ASM) algorithm as defined in [5,6]. If the coarse residual function $\tilde{\mathcal{R}}$ behaves in a similar fashion as the fine residual function $\mathcal{R}$ we now have

$$\frac{\partial \mathcal{K}}{\partial \mathbf{x}} = \frac{\partial \mathcal{P}}{\partial \mathbf{x}} \approx \mathbf{I}, \tag{15}$$

and it is likely that the Quasi-Newton algorithm converges faster when applied to the new rootfinding problem (14). The ASM algorithm consists of two steps:

1. Solve for the coarse fluid-structure interaction solution $\mathbf{z}^*$ as defined in Eq. (11).
2. Apply a Quasi-Newton algorithm to the rootfinding problem as defined in Eq. (14) .

In order to apply the inverse least squares method to approximate the Jacobian $\frac{\partial \mathcal{P}}{\partial \mathbf{x}}$ of the rootfinding problem in step 2, substitute

$$\mathbf{x}^{\text{new}} \in \mathbf{x}^k + \sum_{i=0}^{k-1} c_i^k (\mathbf{x}^i - \mathbf{x}^k) \tag{16}$$

into Eq. (14) and linearize the space mapping function. The result is

$$\mathcal{K}(\mathbf{x}^{new}) = \mathcal{P}(\mathbf{x}^k + \sum_{i=0}^{k-1} c_i^k(\mathbf{x}^i - \mathbf{x}^k)) - \mathbf{z}^* \tag{17}$$

$$\approx \mathcal{P}(\mathbf{x}^k) - \mathbf{z}^* + \left(\frac{\partial \mathcal{P}}{\partial \mathbf{x}}\right) \sum_{i=0}^{k-1} c_i^k(\mathbf{x}^i - \mathbf{x}^k)$$

$$\approx \mathbf{p}^k - \mathbf{z}^* + \sum_{i=0}^{k-1} c_i^k(\mathbf{p}^i - \mathbf{p}^k). \tag{18}$$

The coefficients c_i^k are subsequently found from minimization of the linearized residual $\mathcal{K}(\mathbf{x}^{new})$

$$\mathbf{c}^k = \arg\min_{\mathbf{c}^k \in \mathbb{R}^k} ||\mathbf{p}^k - \mathbf{z}^* + \sum_{i=0}^{k-1} c_i^k(\mathbf{p}^i - \mathbf{p}^k)||, \tag{19}$$

in a least squares sense. The minimization can be performed by the inverse least squares Jacobian approximation given in [4]. We define the difference vectors

$$\begin{cases} \Delta \mathbf{p}^i = \mathbf{p}^i - \mathbf{p}^k \\ \Delta \mathbf{x}_{\mathcal{H}}^i = \mathcal{H}(\mathbf{x}^i) - \mathcal{H}(\mathbf{x}^k), \end{cases} \tag{20}$$

for $i = 0, ..., k-1$. The operator $\mathcal{H}$ in (20) is defined by $\mathcal{H} = \mathcal{S} \circ \mathcal{F}$. We assemble the matrices $\mathbf{V}^k$ and $\mathbf{W}^k$ as

$$\begin{cases} \mathbf{V}^k &= \left[\Delta \mathbf{p}^{k-1}\ \Delta \mathbf{p}^{k-2}\ ...\ \Delta \mathbf{p}^0\right] \\ \mathbf{W}^k &= \left[\Delta \mathbf{x}_{\mathcal{H}}^{k-1}\ \Delta \mathbf{x}_{\mathcal{H}}^{k-2}\ ...\ \Delta \mathbf{x}_{\mathcal{H}}^0\right]. \end{cases} \tag{21}$$

The economy size QR-decomposition of $\mathbf{V}^k$ is used for the Least Squares minimization, that is $\mathbf{V}^k = \mathbf{Q}^k\mathbf{R}^k$. The coefficient vector $\mathbf{c}^k = [c_1^k\ c_2^k\ ...\ c_{k-1}^k]$ is subsequently found from solving

$$\mathbf{R}^k\mathbf{c}^k = \mathbf{Q}^{kT}(\mathbf{z}^* - \mathbf{p}^k). \tag{22}$$

The update $\mathbf{x}^{k+1}$ is then computed from

$$\mathbf{x}^{k+1} \approx \mathbf{x}_{\mathcal{H}}^k + \sum_{i=0}^{k-1} c_i^k(\mathbf{x}_{\mathcal{H}}^i - \mathbf{x}_{\mathcal{H}}^k), \tag{23}$$

which can be written as

$$\mathbf{x}^{k+1} = \mathbf{x}^k + \mathbf{W}^k\mathbf{c}^k + \mathbf{r}^k, \tag{24}$$

where $\mathbf{r}^k = \mathcal{R}(\mathbf{x}^k)$. The Aggressive Space Mapping algorithm with Inverse Least Squares approximation of the Jacobian (ASM-ILS) is summarized in algorithm 1. Each time a space mapping function evaluation is required (in algorithm 1: line 3 and line 19) we use algorithm 2 to solve for $\mathbf{p}^k$. A natural question is whether the ASM-ILS algorithm is more efficient than a Quasi-Newton algorithm – with inverse least squares approximation of the Jacobian – directly applied to $\mathcal{R}(\mathbf{x}) = 0$. Intuitively, this depends on the cost of a coarse residual

evaluation in comparison to the cost of a fine residual evaluation and to what extent equation (15) is satisfied. We will analyze the speedup of the ASM-ILS algorithm in more detail in section 4.

Algorithm 1 ASM - ILS

Require: $\mathbf{x}^0, \mathbf{z}^*, \epsilon_I$
$k = 0$
$\nabla^k_{\mathbf{x}}\mathcal{P} = \mathbf{I}$
$\mathbf{p}^k = \mathcal{P}(\mathbf{x}^k)$
while $||\mathbf{r}^k|| > \epsilon_I$ **do**
  if $k = 0$ **then**
    $\mathbf{x}^{k+1} = \mathbf{x}^k + (\nabla^k_{\mathbf{x}}\mathcal{P})^{-1}(\mathbf{z}^* - \mathbf{p}^k)$
  else
    for $i = 0$ to $k-1$ **do**
      $\Delta\mathbf{x}^i_{\mathcal{H}} = \mathbf{x}^i_{\mathcal{H}} - \mathbf{x}^k_{\mathcal{H}}$
      $\Delta\mathbf{p}^i = \mathbf{p}^i - \mathbf{p}^k$
    end for
    $\mathbf{V}^k = \left[\Delta\mathbf{p}^{k-1}\ \Delta\mathbf{p}^{k-2}\ ...\ \Delta\mathbf{p}^0\right]$
    $\mathbf{W}^k = \left[\Delta\mathbf{x}^{k-1}_{\mathcal{H}}\ \Delta\mathbf{x}^{k-2}_{\mathcal{H}}\ ...\ \Delta\mathbf{x}^0_{\mathcal{H}}\right]$
    Calculate $\mathbf{V}^k = \mathbf{Q}^k\mathbf{R}^k$
    Calculate $\mathbf{R}^k\mathbf{c}^k = \mathbf{Q}^{kT}(\mathbf{z}^* - \mathbf{p}^k)$
    $\mathbf{x}^{k+1} = \mathbf{x}^k + \mathbf{W}^k\mathbf{c}^k + \mathbf{r}^k$
  end if
  $k = k + 1$
  $\mathbf{p}^k = \mathcal{P}(\mathbf{x}^k)$
end while
return $\mathbf{x}^* = \mathbf{x}^k$

Algorithm 2 Evaluating $\mathbf{p}^k = \mathcal{P}(\mathbf{x}^k)$

Require: $\mathbf{x}^k, \mathbf{z}^0, \epsilon_s$
$i = 0$
$\mathbf{r}^k = \mathcal{R}(\mathbf{x}^k)$
$\tilde{\mathbf{r}}^i = \tilde{\mathcal{R}}(\mathbf{z}^i)$
while $||\tilde{\mathbf{r}}^i - \mathbf{r}^k|| > \epsilon_s$ **do**
  $\mathbf{z}^{i+1} = \mathcal{S} \circ \tilde{\mathcal{F}}(\mathbf{z}^i) - \mathbf{r}^k$
  $i = i + 1$
  $\tilde{\mathbf{r}}^i = \mathcal{S} \circ \tilde{\mathcal{F}}(\mathbf{z}^i) - \mathbf{z}^i$
end while
return $\mathbf{p}^k = \mathbf{z}^i$

4. Estimated speedup

The speedup of the ASM-ILS method with respect to the QN-ILS method is determined by the decrease of computational effort per time step to obtain the fine model solution $\mathbf{x}^*$ up to a tolerance ϵ_I.

Let w^i_f and w^j_c be a measure of the cost (flops or CPU time) necessary to evaluate $\mathcal{R}(\mathbf{x}^i)$ and $\tilde{\mathcal{R}}(\mathbf{z}^j)$ respectively. The average cost per time step of a fine and coarse model residual evaluation is then found from

$$w_f = \frac{1}{n_f}\sum_{i=0}^{i=n_f} w^i_f \quad \text{and} \quad w_c = \frac{1}{n_c}\sum_{j=0}^{j=n_c} w^j_c, \tag{25}$$

where n_f and n_c are the total number of fine and coarse residual evaluations respectively (including the iterations necessary to find $\mathbf{z}^*$) per time step. The total cost per time step of the ASM-ILS method is subsequently estimated by

$$W^A \approx w^A_f n^A_f + w^A_c n^A_c, \tag{26}$$

whereas the total cost of the QN-ILS method is estimated by

$$W^Q \approx w^Q_f n^Q_f. \tag{27}$$

In Eq. (26) and (27), the superscript A refers to a quantity associated with the ASM-ILS algorithm and the superscript Q refers to a quantity accociated with the QN-ILS algorithm. The

estimates in Eq. (26) and (27) are based on the premise that the largest part of the computational effort is spent to evaluate the coarse and fine residuals in the computation, neglecting all other (overhead) costs. Numerical experiments justify this premise. The estimated speedup per time step is then given by

$$S_p \approx \frac{W^Q}{W^A} = \frac{n_f^Q}{n_f^A + \frac{w_c^A}{w_f^Q} n_c^A}, \tag{28}$$

where we have used that $w_f^A \approx w_f^Q$.

The ASM-ILS method is more efficient than the QN-ILS method if $S_p > 1$. The speedup becomes insensitive to the number of coarse residual evaluations n_c^A if the ratio $\frac{w_c^A}{w_f^Q}$ is sufficiently small. The choice for the inner iterative method is not that important in this case as long as it results in a stable algorithm for the evaluation of the space mapping function. To obtain a metric of the total speedup of a simulation we define

$$\hat{S}_p \approx \frac{\sum W^Q}{\sum W^A}, \tag{29}$$

where the sum is taken over all the time steps in the numerical integration.

5. Numerical test case and results

In this section the ASM-ILS algorithm will be applied to a simple academic test problem – the supersonic panel flutter problem – in order to assess the speedup as defined in section 4. To this end, a structure model, fine fluid model en coarse fluid model are defined in section 5.1, 5.2 and 5.3 respectively. Finally, numerical experiments are performed in section 5.4 in order to investigate the influence of physical parameters and time step sizes on the speedup of the ASM-ILS algorithm.

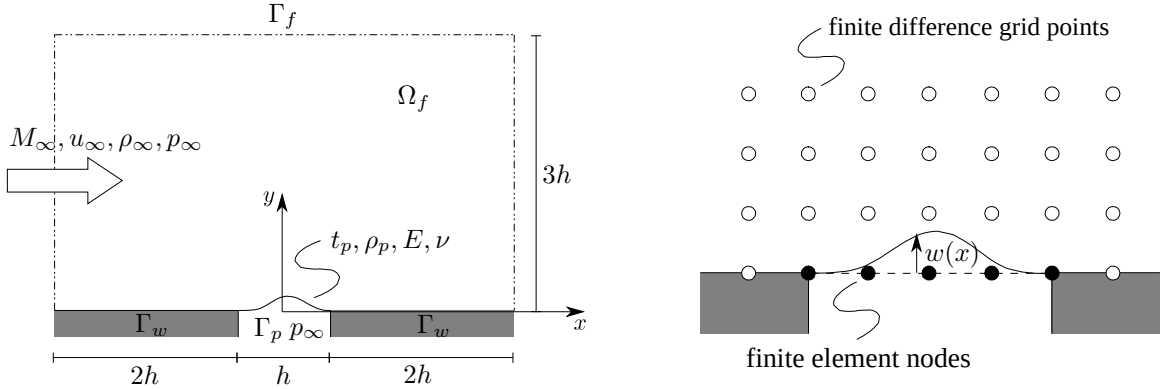

Figure 1. Schematic representation of the panel flutter problem

5.1. Structure model

The flexible panel is governed by the Euler Bernoulli beam equation

$$\begin{cases} \rho_p t_p \frac{\partial^2 w}{\partial t^2} + \frac{\partial^2}{\partial x^2}\left[\frac{EI}{1-\nu^2}\frac{\partial^2 w}{\partial x^2}\right] = -\Delta p(x) \quad (x) \in \Gamma_p, \\ w(\pm\frac{h}{2}) = \frac{\partial w}{\partial x}(\pm\frac{h}{2}) = 0, \end{cases} \tag{30}$$

In Eq. (30), ρ_p denotes the density of the panel, t_p the thickness of the panel, E the Youngs modulus, ν Poisson's ratio, $I = \frac{1}{12}t_p^3$ the moment of inertia and w the vertical panel displacement. The forcing term is given by the pressure difference over the panel

$$\Delta p = p_I(x) - p_\infty \quad (x) \in \Gamma_p, \tag{31}$$

where p_I denotes the pressure of the fluid on the fluid-structure interface Γ_p and p_∞ the freestream pressure, see figure 1. The boundary value problem (30) is discretized using the finite element method with Hermitian shape functions such that the nodal unknowns are displacements *and* rotations.

5.2. Fine fluid model

The high fidelity fluid is governed by the two-dimensional unsteady linearized potential equation

$$\begin{cases} \nabla^2\phi - \frac{1}{a_\infty^2}\frac{D}{Dt}\left(\frac{D\phi}{Dt}\right) = 0 & \text{in } \Omega_f, \\ \phi(x,y) = 0 & \text{on } \Gamma_f, \\ v(x,y) = 0 & \text{on } \Gamma_w, \\ v(x,y) = \frac{Dw}{Dt} & \text{on } \Gamma_p, \end{cases} \tag{32}$$

where ϕ denotes the perturbed fluid potential and M_∞ and a_∞ are the freestream Mach number and freestream fluid speed of sound. The substantial derivative in (32) is given by

$$\frac{D}{Dt} = \frac{\partial}{\partial t} + M_\infty a_\infty \frac{\partial}{\partial x} \quad (x,y) \in \Omega_f. \tag{33}$$

The linearized potential equation is valid for subsonic flow and supersonic flow but is not applicable in the transonic regime. The horizontal velocity compononent u and vertical component v of the fluid are recovered from the potential according to

$$u = u_\infty + \frac{\partial\phi}{\partial x} \quad \text{and} \quad v = \frac{\partial\phi}{\partial y} \quad (x,y) \in \Omega_f. \tag{34}$$

The interface pressure on top of the panel is given by Bernoulli's equation [11]

$$p_I(x) = p_\infty - \rho_\infty \frac{D\phi}{Dt} \qquad (x) \in \Gamma_p. \tag{35}$$

The fluid boundary value problem (32) is discretized using the finite difference method. The finite difference grid conforms with the finite element mesh of the panel.

5.3. Coarse fluid model

Using the piston analogy model (see [12]), the interface pressure is approximated by

$$p_I(x) = p_\infty + \rho_\infty M_\infty a_\infty \left(\frac{M_\infty^2 - 2}{\sqrt{(M_\infty^2 - 1)^3}} \frac{\partial w}{\partial t} + M_\infty a_\infty \frac{\partial w}{\partial x} \right) \qquad (x) \in \Gamma_p. \tag{36}$$

The piston analogy is valid for $M_\infty > 1.6$. The pressure in Eq. (36) directly depends on the deflection of the panel. The computational effort is therefore negligible compared to the use of the fine fluid model.

5.4. Numerical experiments

The similarity parameters are the Mach number M_∞, the fluid-to-structure mass ratio ζ and the ratio of characteristic time-scales λ defined by

$$\zeta = \frac{\rho_\infty L}{\rho_p t_p} \quad \text{and} \quad \lambda = \frac{La_\infty^{-1}}{(\rho_p t_p)^{1/2} L^2 (EI)^{-1/2}}. \tag{37}$$

The values of these parameters – for each test case under consideration – are collected in table 1. Linear stability analysis is used to obtain the critical Mach number, i.e. the Mach number which separates the stable from the unstable regime. The critical Mach number $M_{cr} = 2.27$ and circular frequency $\omega_{cr} = 460\ rad/s$ of test case FSI-1 agree with the values reported in [12].

Test case	M_{cr}	ζ	λ
FSI-1	2.27	$5.47e^{-2}$	$1.47e^{-2}$
FSI-2	2.28	$7.41e^{-2}$	$1.47e^{-2}$
FSI-3	2.33	$3.00e^{-1}$	$1.47e^{-2}$

Table 1. Similarity parameters of the 2-D FSI test cases

The Newmark-β time integration scheme is used to integrate the structure and fluid equations of motion. This scheme is known to be second order accurate and unconditionally stable for $\gamma = 1/2$ and $\beta = 1/4$. We use the a-form implementation, see [13].

The panel is released from an initial displacement equal to the fluttermode $w^0 = 0.1\xi$, see figure 2. The corresponding steady fluid potential ϕ is depicted in figure 3. The simulations are performed at the critical Mach numbers M_{cr}. The observed frequency ω_{cr} in the simulation is then equal to the critical frequency obtained by linear stability analysis. The nondimensional coupled period $P_{cr} = 2\pi a_\infty / \omega_{cr} L$ is divided in 10, 30 and 70 time steps for each test case to study the influence of the time step on the speed up. The coupled periods of test case FSI-1, FSI-2 and FSI-3 are $P_{cr}^1 = 8.2$, $P_{cr}^2 = 7.0$ and $P_{cr}^3 = 3.5$ respectively. The numerical parameters used in the simulations are assembled in table 2. The fluid grid size and number of finite elements in table 2 correspond to a test case used in [15].

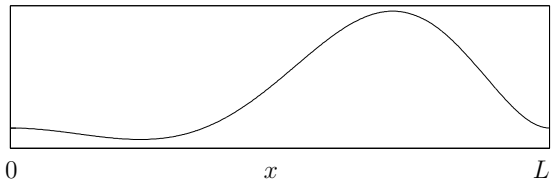

Figure 2. Initial panel deflection $w^0 = 0.1\xi$.

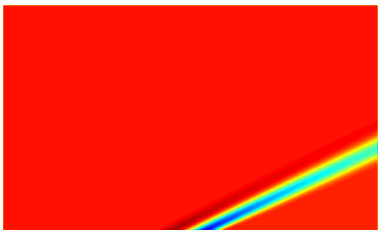

Figure 3. Steady initial fluid field.

Description	symbol	value
Fluid grid size	$N_x \times N_y$	321×193
Number of Finite Elements	N_e	129
Number of time steps	N_t	$20 \cup 60 \cup 140$
Time step	Δt	$2P_{cr}/N_t$
Outer tolerance	ϵ_I	$1 \cdot 10^{-6}$
Inner tolerance	ϵ_s	$1 \cdot 10^{-7}$

Table 2. Numerical parameters

An inner product of the panel displacement with the flutter mode is defined by

$$a_g(t) = \frac{1}{\int_0^L \xi^2(x)dx} \int_0^L \xi(x)w(x,t)dx. \tag{38}$$

The inner product is used to plot the time history of the panel after it is released from its initial deflection. An example is given in figure 4 which shows the fine and coarse model responses. Both responses demonstrate that the panel oscillates in the flutter mode at the predicted frequency $\omega_{cr} = \frac{2\pi a_\infty}{LP_{cr}} = 539 rad/s$.

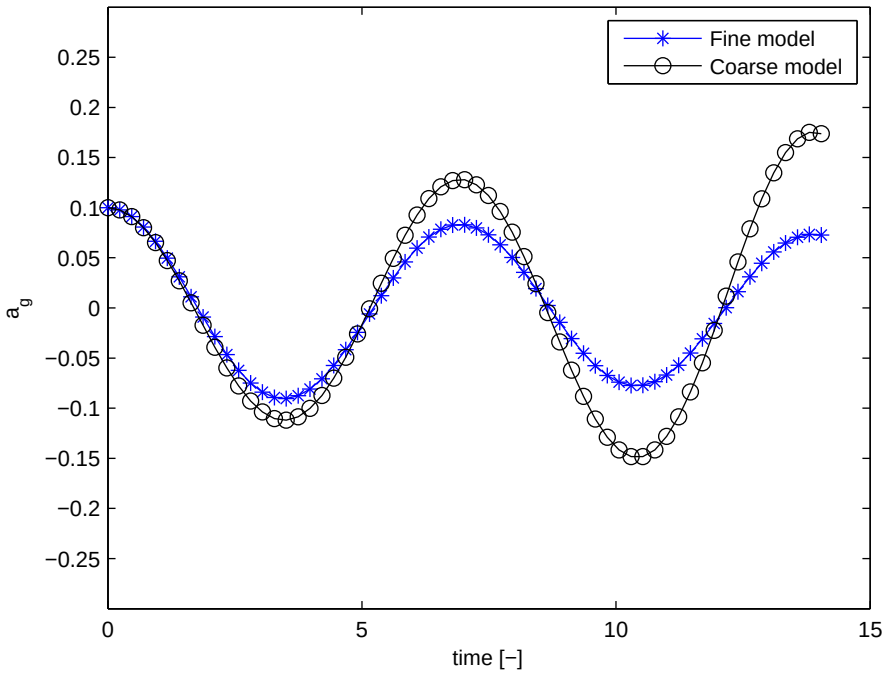

Figure 4. Panel response a_g for test case FSI-2 with $\Delta t = P_{cr}^2/30$.

Figure 5 shows the interface residual convergence for a chosen representative time step of the simulation. It can be seen that the ASM-ILS algorithm outperforms the QN-ILS algorithm when we choose the convergence criterion $\epsilon_I = 1 \cdot 10^{-6}$. An improvement is already visible after the first iteration and becomes better with the adaption of the space mapping Jacobian.

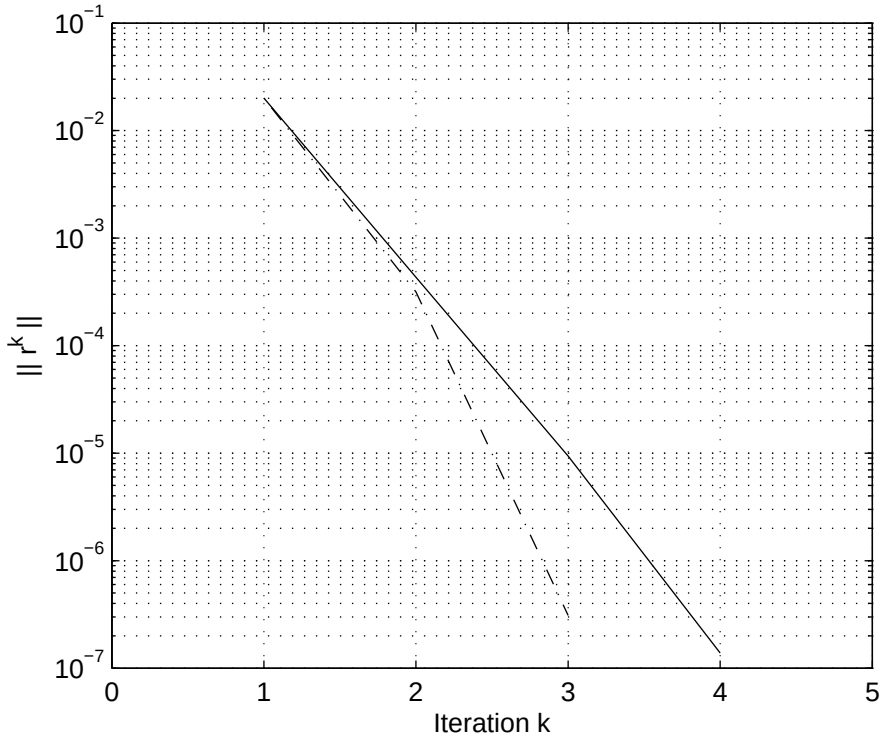

Figure 5. Interface residual convergence during a representative time step of test case FSI-2, $\Delta t = P_{cr}^2/30$. QN-ILS algorithm (-), ASM-ILS algorithm (- · -) .

The estimated speedup per time step is shown in figure 6. The speedup is around $S_p \approx \frac{n_f^Q}{n_f^A} = \frac{4}{3}$ for most time steps in the simulation since $\frac{w_c}{w_f}$ is negligible, see figure 7.

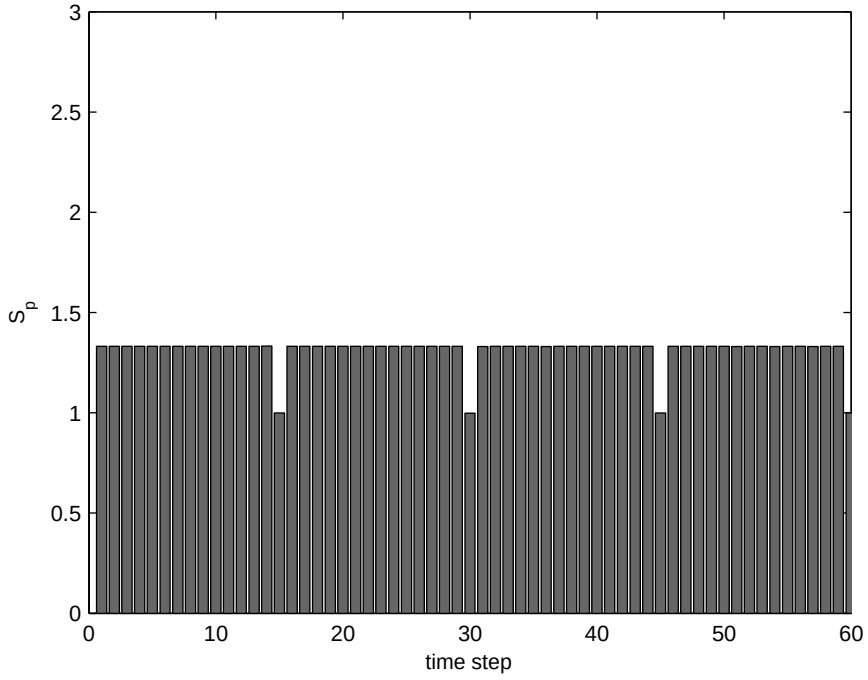

Figure 6. Estimated speedup per time step, test case FSI-2 with $\Delta t = P_{cr}^2/30$.

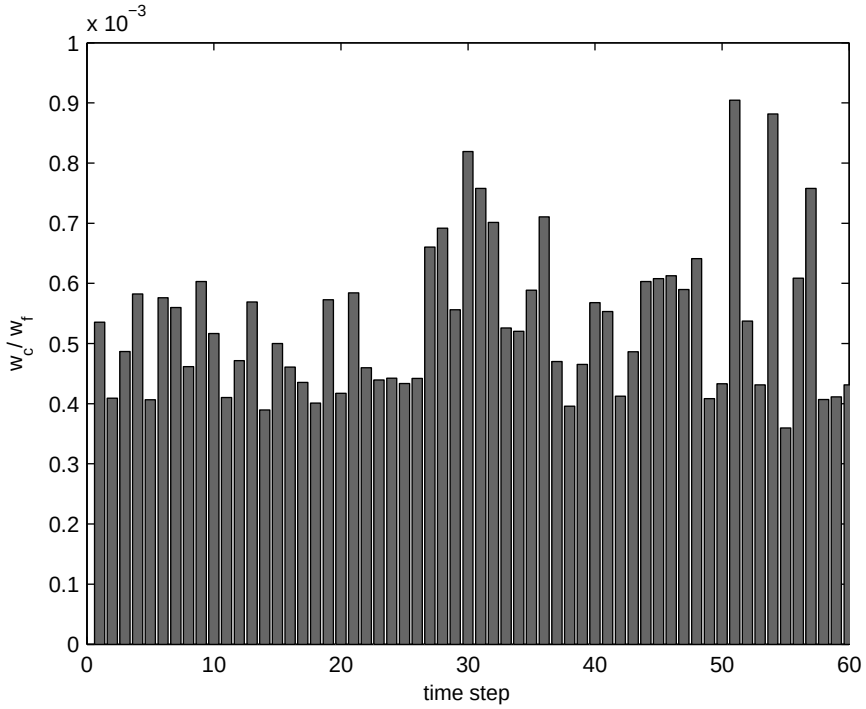

Figure 7. Average work ratio per time step, test case FSI-2 with $\Delta t = P_{cr}^2/30$.

Table 3 lists the total speedup of the simulations using different time step sizes. The influence of the time step size is large and demonstrates that no speedup is obtained when the time step size becomes too small. In this case only 3 iterations are sufficient to converge and it becomes difficult to obtain a speedup larger than 1. In contrast to fluid-structure interaction problems involving incompressible fluids the added mass effect is not causing problems when small time steps are considered. The speedup obtained with the ASM-ILS method is therefore limited in this case. The influence of the physical parameters on the speedup achieved with the ASM-ILS algorithm is surprisingly small. This requires further investigations.

Test case	$\Delta t = P_{cr}/10$	$\Delta t = P_{cr}/30$	$\Delta t = P_{cr}/70$
FSI-1	$1.56\ (\approx 6/4)$	$1.30\ (\approx 4/3)$	$1.28\ (\approx 4/3)$
FSI-2	$1.54\ (\approx 6/4)$	$1.31\ (\approx 4/3)$	$0.998\ (\approx 3/3)$
FSI-3	$1.44\ (\approx 6/4)$	$1.30\ (\approx 4/3)$	$0.999\ (\approx 3/3)$

Table 3. Estimated total speedup $\hat{S}_p$ of the simulations .

Table 4 shows the observed speedup measured by the total CPU time ratio. Slightly lower efficiencies are measured due to the overhead costs which are higher for the ASM-ILS algorithm than for the QN-ILS algorithm. The CPU time ratios listed in table 4 fluctuate for constant parameter settings. The estimated total speedup from table 3 therefore yields a better efficiency metric for comparison.

Test case	$\Delta t = P_{cr}/10$	$\Delta t = P_{cr}/30$	$\Delta t = P_{cr}/70$
FSI-1	1.44	1.23	1.29
FSI-2	1.45	1.19	0.95
FSI-3	1.29	1.19	0.97

Table 4. Observed speedup of the simulations .

6. Conclusion

We develop a new coupling algorithm for the efficient simulation of fluid-structure interaction using the Aggressive Space Mapping (ASM) technique. The space mapping technique exploits a computationally cheap low-fidelity fluid model in order to accelerate the subiteration process necessary to find the solution of an expensive high fidelity fluid model using black-box information only. We use the inverse least squares algorithm to approximate the space mapping Jacobian and define the speedup as the ratio of the computational work necessary in the QN-ILS algorithm divided by the computational work necessary in the ASM-ILS algorithm.

The observed speedup is 1–1.5 and depends strongly on the time-step size. No speedup is obtained by the ASM-ILS algorithm when the time step becomes too small. This can be explained by the fact that a compressible fluid model is used which lacks the problem of *added mass* when the time step size decreases. From this observation it is expected that the ASM-ILS algorithm performs better at small time step sizes when the structure is in interaction with an incompressible fluid. In future research we would like to: (1) include a non-linear high fidelity fluid model; (2) study the performance of the algorithm when incompressible fluid dynamics is used; (3) study the influence of the use of different low-fidelity fluid models on the speedup obtained by the space mapping algorithm.

The results motivate to continue the development of space mapping algorithms for the efficient simulation of strongly coupled fluid-structure interaction problems.

Acknowledgements

The research leading to these results has received funding from the European Community's Seventh Framework Programme (FP7 / 2007-2013) under grant agreement number 233665. FFAST (Future Fast Aeroelastic Simulation Technologies) is a collaborative research project aimed at developing, implementing and assessing a range of numerical simulation technologies to accelerate future aircraft design. Advances in critical load identification and reduced order modelling methods will potentially provide a step change in the efficiency and accuracy of the dynamic aeroelastic loads process. The partners in FFAST are: University of Bristol, INRIA, CSIR, TU Delft, DLR, IRIAS, University of Liverpool, Politecnico di Milano, NUMECA, Optimad Engineering, Airbus-UK, EADS-MS and IITP.

7. REFERENCES

[1] Y. Bazilevs, J.R. Gohean, T.J.R. Hughes, R.D. Moser and Y. Zhang, "Models and Methods in Computational Vascular and Cardiovascular Mechanics". *Computer Methods in Applied Mechanics and Engineering*, 45-46 (2012), 3534–3550.

[2] J. Degroote, J. Vierendeels, "Multi-solver algorithms for the partitioned simulation of fluid–structure interaction". *Computer Methods in Applied Mechanics and Engineering*, 200 25-28 (2011), 2195–2210.

[3] C. Michler, H. van Brummelen, R. de Borst, "An investigation of Interface-GMRES(R) for fluid–structure interaction problems with flutter and divergence". *Computational Mechanics*, 47 (2011), 17–29.

[4] J. Degroote, K-J. Bathe, J. Vierendeels, "Performance of a new partitioned procedure versus a monolithic procedure in fluid–structure interaction". *Computers and Structures*, 87 11-12 (2009), 793–801.

[5] D. Echeverría, and P.W. Hemker, "Space Mapping and defect correction". *Computational Methods in Applied Mathematics*, 5 2 (2005), 107–136.

[6] J.W. Bandler, R.M. Biernacki, S.H. Chen, R.H. Hemmers, K. Madsen, "Electromagnetic optimization exploiting aggressive space mapping". *Microwave Theory and Techniques, IEEE Transactions on*, 43 (1995), 2874–2882.

[7] H.G. Matthies, R. Niekamp, J. Steindorf, "Algorithms for strong coupling procedures". *Computer Methods in Applied Mechanics and Engineering*, 195 17-18 (2006), 2028–2049.

[8] S. Minami, S. Yoshimura, "Performance evaluation of nonlinear algorithms with line-search for partitioned coupling techniques for fluid-structure interactions". *International Journal for Numerical Methods in Fluids*, 64 (2010), 1129–1147.

[9] T.P. Scholcz, A.H. van Zuijlen, H. Bijl, "A multi-model incremental adaptive strategy to accelerate partitioned fluid-structure algorithms using space-mapping". *IV International Conference on Computational Methods for Coupled Problems in Science and Engineering (Coupled Problems 2011), 20-22 June 2011, Kos, Greece*, Barcelona: International Center for Numerical Methods in Engineering (CIMNE).

[10] T. Gallinger, K. Bletzinger, "Comparison of algorithms for strongly coupled partitioned fluid-structure interaction". *IV International Conference on Computational Methods for Coupled Problems in Science and Engineering (Coupled Problems 2011), 20-22 June 2011, Kos, Greece*, Barcelona: International Center for Numerical Methods in Engineering (CIMNE).

[11] E.H. Dowell, Aeroelasticity of plates and shells, Noordhoff International Publishing, Leiden, fourth edition, 1975

[12] S. Piperno, C. Farhat, "Partitioned procedures for the transient solution of coupled aeroelastic problems - Part II: energy transfer analysis and three-dimensional applications". *Computer Methods in Applied Mechanics and Engineering*, 190 24-25 (2001), 3147–3170.

[13] T.J.R. Hughes, The Finite Element Method, Prentice-Hall, 1987.

[14] J.W. Bandler, R.M. Biernacki, S.H. Chen, P. A. Grobelny, R.H. Hemmers, "Space mapping technique for electromagnetic optimization". *IEEE Transactions on Microwave Theory and Techniques*, 42 (1994), 2536–2544.

[15] C.V. Verhoosel, T.P. Scholcz, S.J. Hulshoff, M.A. Gutiérrez, "Uncertainty and reliability analysis of fluid-structure stability boundaries". *AIAA Journal*, 47 (2009), 91–104.